Mathematical Modelling of Pool Fire Burning Rates in a Full-Scale Ventilated Tunnel

Hui Ying WANG and Hatem SAHRAOUI
Institut P', Fluides-Thermique-Combustion
CNRS-UPR3346, ENSMA, Université de Poitiers, BP 40109 F86961 Futuroscope Chasseneuil Cedex, France

ABSTRACT

A computational fluid dynamic model with full coupling between gaseous and liquid phases is developed to predict buring rates of liquid pool fires in ventilated full-scale tunnel. Rates of fuel release are calculated using predictions of flame feedback to the surface of the pool. A pool fire in tunnel is modelled as an unsteady process, from the time of ignition until convergence to a quasi-steady burning rate. This feedback supports sustained flame above the pool surface and controls the burning rate of the fuel. The numerical model solves three dimensional, time-dependent Navier-Stokes equations, coupled with submodels for soot formation and thermal radiation transfer. Turbulent combustion process is modelled by an Eddy Dissipation Concept (EDC) by using two chemical reaction steps to CO prediction. The numerical model is shown to possess the ability to predict the effect of ventilation on burning rate and the initial growth period in a full-scale tunnel fire. The current study indicates that CO generation is relatively independent of position in the overfire region, and correlated solely as a function of mixture fraction. While no correlation of soot concentrations in terms of the mixture fraction is found. Abundant CO and soot are formed around the fire base, which is later deflected near the tunnel ceiling, and the backflow brings about the toxic products with a noticeable smoke stratification as the airflow velocity is below a critical value.

KEYWORDS: tunnel fire modelling, CFD, backlayering flow, heat flux, toxicity

INTRODUCTION

The present study is motivated by the interest in fire safety science of tunnels following the increasing number of catastrophic tunnel fires and the increasing number of tunnels built. In under-ventilated tunnel fires, existence of reverse stratified layer of hot combustion products against a cross-stream has an important bearing on fire fighting and evacuation. The critical velocity, required to suppress the backlayering flow upstream of the fire section in the tunnel, is the most well investigated fire phenomenon [1-2]. The work of Vauquelin [3] shows that for large values of Heat Release Rate (HRR), the dimensionless critical velocity becomes independent of the HRR. Effort has been also put into analyzing flame length, due to flame impingement in tunnel, which is the primary mode of fire spread from one object to another through radiant feedback from the hot gases. Rew and Deaves [4] presented an empirical expression for the effects of wind velocity and heat release rate on the flame length, but the tunnel width or height was not included. Through an analysis of fire spread during large-scale fire tests, Lönnermark and Ingason [5] show that the longitudinal ventilation shortens the flame length as the velocity increases. An increasing number of numerical study for full-scale tunnel fires is also found. Fletcher et al. [6] carried out a three dimensional simulations of a full-scale mock-up of a mine roadway. Woodburn and Britter [7] indicated that the whole tunnel fire would have to be simulated. Hwang and Edwards [8] concluded that the levelling-off of the critical ventilation velocity as the fire heat generation increases is solely due to the temperature maximum above the fire source.

A high number of fatalities in tunnel is due to the toxicity of smoke particulates and gases from the fire. Carbon monoxide, a smoke component which is the yields of incomplete combustion, augments the overall toxicity of these products to a great extent [9]. The problem of carbon monoxide production in enclosure fires has been largely studied, and important outcomes are described by Gottuk [10]. No correlations and model were proposed. The correlation between the emissions of carbon monoxide and soot is important because they both are major contributors to hazards [11]. It also underlies Orloff success [12] in correlating concentration of CO in terms of the local average mixture fraction. Most of the previously developed soot [13] and CO models are impractical for use in a full-scale tunnel fire due to their complexity, computational cost, or large number of fuel-specific parameters that are not easily obtained. A fire model's treatment of soot formation has a profound influence on reliably predictions of mass burning of condensed fuels, flame

spread and fire growth through thermal radiation. There is currently no entirely tractable solution for engineering calculations.

In the work of Floyd [14], the yields of CO and soot should be specified for the combustion model. The simplified combustion and soot models often have problems with simulating under-ventilated large-scale tunnel fire in a good way. With this motivation, a two-step combustion model and smoke-point model are embedded within a FDS5 code [14] and used for a comparison of predicted and measured temperatures, soot volume fraction and chemical species. The model will also work in the similar FDS6 code. The authors used the current (EDC) combustion model to simulate the tunnel fires and compare their results with the mixture fraction model [14] and experiments [15]. By using EDC, the abundant CO formed around the fire base is deflected near the ceiling, and the backlayering flow brings about the more toxic products with presence of a noticeable smoke stratification. However, by using mixture fraction model with a specified CO yield, CO production enters rapidly the decay phase away from the fire source. This is the subject of the paper where a soot model based on the smoke point [16] is introduced and used to calculate soot formation in non-premixed turbulent flames of several fuels. We have attempted to develop a model for soot formation and CO that considers only the phenomena essential for obtaining sufficiently accurate predictions of soot and CO concentrations.

THEORETICAL ANALYSIS

This section outlines the physico-mathematical representation of the reacting flow phenomena of interest here. The basis of the analysis is the conservation equations of mass, momentum, energy and species, a set of three-dimensional, time-dependent Navier-Stokes equations. The finite-difference technique is used to discretize the partial differential equations [14], which are solved through an elliptic solver. The gas temperature on filtering scale is used in the Arrhenius rate laws for soot formation and CO to CO_2 conversion.

Subgrid Kenetic Energy

In Large Eddy Simulation (LES), the Sub-grid scale (SGS) kinetic energy represents the unresolved turbulent energy and needs to be modelled. The subgrid kinetic energy, k, is solved by a transport equation, and its basic form was inspired by the work of Menon [17].

$$\frac{\partial \rho k}{\partial t} + \frac{\partial (\rho u_i k)}{\partial x_j} = \frac{\partial}{\partial x_j}\left(\mu_t \frac{\partial k}{\partial x_j}\right) - \tau_{ij,SGS}\frac{\partial u_i}{\partial x_j} - \rho \varepsilon \qquad (1)$$

Here ρ is the density and μ_t the eddy viscosity from the analysis of Smagorinsky [14] on the resolved field. The terms on the right side of equation represent, respectively, the transport, the production and the dissipation of subgrid kinetic energy. The production terms is determined from the shear stresses, $\tau_{ij,SGS}$, which are evaluated from the resolved dynamic field. No transport equation of dissipation rate is solved, and its value is determined from a characteristic grid size, Δ, and the SGS kinetic energy as below :

$$\varepsilon = c_\varepsilon \frac{k^{3/2}}{\Delta} \qquad \text{with} \qquad c_\varepsilon = 0.7 \qquad (2)$$

Combustion Via Two Chemical Reaction Steps

The combustion processes are governed by the convection-diffusion equations for the mass fraction, Y_i, of the six major chemical species, such as C_mH_n, O_2, CO, CO_2, H_2O and N_2. The mixing-controlled combustion via two chemical reaction steps for CO formation, is assumed.

$$C_mH_n + \left(\frac{m}{2} + \frac{n}{4}\right)O_2 \rightarrow mCO + \frac{n}{2}H_2O \qquad (3)$$

$$CO + \frac{1}{2} O_2 \rightarrow CO_2 \tag{4}$$

The combustion rate is assumed to be controlled by the eddy mixing rate with which the local reaction rates of fuel and CO, are calculated from an EDC.

$$\dot{\omega}_i = \rho \frac{d Y_i}{dt} = -\rho \tau_{mix} min(Y_i, \frac{Y_{O2}}{v_{g,i}}) \tag{5}$$

where $v_{g,i}$ denotes the stoichiometric coefficient, and Y_i the fuel/CO mass fractions. Regarding the chemical reaction time, one need only consider the first step (3) of as being instantaneous. The second step (4) is much slower than the first step, and the oxidation rate of CO is also determined from an Arrhenius expression [18],

$$\dot{\omega}_{CO,ARR} = -A \, exp(-E / RT)[CO][H_2O]^{0.5}[O_2]^{0.25} \tag{6}$$

This over-all rate expression (6) for carbon monoxide-oxygen reaction is established from a turbulent flow reactor in the presence of water. The local reaction rate of CO is crudely accounted for with the slower rate of the mixing rate (Eq.5) and the Arrhenius rate (Eq.6). The heat release rate is determined from the consumption rate of the two combustibles of CO and C_mH_n. This combustion model in non-premixed flames is made tractable by their inherent simplicity.

The postulated model deviates from the resolved view of reaction because processes of turbulent energy cascade are not explicitly considered. In most fires, the primary momentum transport of turbulent diffusion flame is sustained by large-scale energy-containing eddies [19] which are related to a typical geometry characteristic of a pool fire. Simplicity is achieved by the recognition that reaction in pool-like fire is controlled by the diffusion of oxygen into the reactive zone in a resolved scale rather than being limited by Kolmogorov time scale. The key timescales, τ_{mix}, is supposed to relate approximately to the dissipation rate.

$$\tau_{mix} \approx C_{EDC} \frac{\varepsilon}{k} \tag{7}$$

The heat generation resulting from the dissipation of turbulence energy is assumed to mainly occur on the SGS where production and dissipation balance. In the present study, we apply the dynamic modelling method to obtain appropriate value of the coefficient C_{EDC}.

$$C_{EDC} = 23.6 \left(\frac{v\varepsilon}{k^2} \right)^{1/4} \frac{\chi}{1 - \chi\gamma} \tag{8}$$

where γ is the fraction of the fluid contained within the fine structures [20].

$$\gamma = 9.7 \left(\frac{v\varepsilon}{k^2} \right)^{3/4} \tag{9}$$

Here χ is a factor between zero and one to express the fraction of the fine structures which can react as a function of the mixture fraction, Z.

$$\chi = \frac{Z}{Z_{st}} \ \ if \ 0 \le Z < Z_{st} \ \ and \ \ \chi = \frac{1-Z}{1-Z_{st}} \qquad if \ \ Z_{st} \le Z \le 1 \tag{10}$$

where Z_{st} is the stoichiometric mixture fraction. The dynamic modelling method in terms of k, ε and the kinematic viscosity ν, allows to take into account the mass transfer rate between the fine structures and the bulk of the fluid.

Radiative Heat Transfer

For a heavily sooting flame such as fire, radiation is a crucial aspect of combustion, and can dominate other modes of heat transfer. A radiative transfer equation (RTE) is solved by using a discrete expression adapted to a finite volume method [14].

$$\vec{\nabla}.\vec{\Omega}I + \kappa I = \kappa \frac{\sigma T^4}{\pi} \tag{11}$$

As the radiation spectrum of soot is continuous, it is assumed that the mixture of soot and gas behaves as a gray medium with a mean absorption coefficient, κ, used in RTE. For simplicity, six bands are selected to give an accurate representation of the most important radiation bands of CO_2 and H_2O. For the calculation of the gray or band-mean gas absorption coefficient, κ_g, a narrow-band model (RadCal) has been implemented in FDS5 [14]. The coupling of combustion and soot can not be accounted for. The effect of soot concentration on radiation is included by adding the radiation coefficient of soot, κ_s, into that of gas.

$$\kappa = \kappa_s + \kappa_g \tag{12}$$

where soot absorption coefficient is calculated as a function of the temperature, T, and soot volume fraction, f_v [16] :

$$\kappa_s = 1225 f_v T \qquad with \qquad f_v = \frac{\rho Y_s}{\rho_{soot}} \tag{13}$$

Soot Formation and Its Oxidation

A global soot formation model is incorporated into a turbulent flow calculation in a convection-diffusion equation for the soot mass fraction, Y_s.

$$\frac{\partial \rho Y_s}{\partial t} + \frac{\partial (\rho u_i Y_s)}{\partial x_j} - \frac{\partial}{\partial x_j}\left(\frac{\mu_t}{Sc_t} \frac{\partial Y_s}{\partial x_j} \right) = \dot{\omega}_s \tag{14}$$

The soot production rate is written as :

$$\dot{\omega}_s = \begin{cases} \dot{\omega}_f - \dot{\omega}_O & (Z \in [Z_{so}, Z_c]) \\ -\dot{\omega}_O & (Z \in [0, Z_{so}]) \end{cases} \tag{15}$$

Two mixture fraction limits delimit the soot formation and oxidation regions. The incipient mixture fraction is Z_c=0.15, and the mixture fraction threshold where soot oxidation starts is Z_{so}=0.1. A fuel's smoke point is the maximum height of its laminar flame burning in air at which soot is not release from the flame tip. Based on a LSP (Laminar Smoke Point) concept [16], soot formation is assumed to be controlled by second-order homogeneous gaseous reaction processes, and thus, is expressed as a function of the mixture fraction, Z, and gas temperature, T :

$$\dot{\omega}_f = A_f \, \rho^2 \left(\frac{Z - Z_{st}}{1 - Z_{st}} \right) T^\gamma \, exp(-T_\alpha / T) \tag{16}$$

Here the temperature exponent $\gamma = 2.25$ and the activation temperature $T_\alpha = 2000 \, K$. The parameter defining the fuel's sooty propensity is the pre-exponential factor, A_f, which is in reversely proportional to its LSP height. It is not necessary to establish fuel-specific model constants because the smoke point height has been measured for many fuels [16].

The soot oxidation in Eq.(15) is assumed to proceed through a single reaction step,

$$C_s + O_2 \to CO_2 \tag{17}$$

By assuming that the mixing time in sub-grid scale is the limiting mechanism, the specific rate of soot oxidation in turbulent flames is expressed by an EDC approach.

$$\dot{\omega}_o = \rho \, \tau_{mix} \, min(Y_s, \frac{Y_{O2}}{v_s}) \tag{18}$$

where v_s denotes the stoichiometric coefficient for burning 1 kg soot. This model contains no mechanism to suppress homogeneous soot formation by OH and O.

Phase Coupling Conditions

The condensed fuel is assumed to be thermally-thick, a one-dimensional heat conduction equation for the material temperature is solved. The surface temperature, T_s, is affected by gains and losses with the heat balance across the interface :

$$-k_l \frac{d T_s}{dn} = \dot{q}''_{conv} + \dot{q}''_{rad} - \dot{m}''_s L_v \tag{19}$$

Here, k_l is the liquid thermal conductivity and L_v the fuel latent heat. Flame radiation flux, $\dot{q}''_{rad}$, is computed from a discrete representation of the radiative intensity equation (11). The viscous sublayer are critically dependent on the near-wall model due to important viscous effects. An extremely small grid size (mm) is required to fully resolve the turbulent cascade in boundary layer for the high Reynolds number flow, making practical fire simulations difficult. In the present work, the computational nodes immediately adjacent to a wall are located in the fully turbulent region and this simplicity allows faster computations and by this a higher spatial discretization and an increase of the resolved part of the fire oscillation. Predictions of the most dominant radiative heat transfer are generally less sensitive to the near-wall turbulence model. A wall-damping is treated by using a wall function for convective heat feedback due to the coarse meshes used here. The Couette flow is assumed to prevail near the wall surface, and the convective heat feedback is calculated from a wall function [21] far away from the wall for viscous effects to be negligible, that is, at $y^+ \geq 11$.

$$\dot{q}''_{conv} = \frac{(T_g - T_s)\rho \, c_{pg} C_\mu^{1/4} k^{1/2}}{Pr \left[\frac{1}{\kappa} ln(E \, y^+) + P \right]} \tag{20}$$

Here C_μ and E (=9) are the constants in logarithmic law of the wall, κ (=0.41) is the von Karman constant and P an empirical function [21] determined from the ratio between the laminar Prandtl number (Pr=0.7) and turbulent one (Pr$_t$=0.5).

Based on a quasi-steady assumption, the liquid pool vaporization rate, $\dot{m}_s^{''}$, can be derived from the combination of the species and energy equations [22], and expressed as follows :

$$\dot{m}_s^{''} = \frac{\rho\alpha}{l} 0.037\, Re^{4/5}\, Pr^{1/3}\, ln(\,B+1\,) \tag{21}$$

where α is the thermal diffusivity and Re the Reynolds number. The local length scale, l, is attached to the mesh size of the computational nodes immediately adjacent to a liquid surface. Without combustion, the mass transfer number, B, is defined from the mass fraction of liquid equilibrium vapour, $Y_{F,s}$, which is obtained from Clausius-Clapeyron equation [22].

$$B = \frac{Y_{F,g} - Y_{F,s}}{Y_{F,s} - 1} \tag{22}$$

Once ignition occurs due to the mixing between the fuel vapour and air, the mass transfer number, B, is defined from the heat of combustion, H_c.

$$B = \frac{H_c v_{F/o} Y_O + c_{pg}(\,T_g - T_s\,)}{L_v + c_{pl}(\,T_s - T_0\,)} \tag{23}$$

where $v_{F/o}$ is the stoichiometric fuel/oxygen ratio and L_v the heat of vaporization. The mass transfer number is also dependent on the length scale through the local fuel/oxygen mass fraction, $Y_{F,g}/Y_O$, and temperature, T_g, in hot free stream gas near the liquid surface. Predictions of the liquid pool vaporization rate are generally less sensitive to the length scale due to the associated mass transfer number.

RESULTS AND DISCUSSION

This 3D tunnel geometry and the coordinate system for numerical simulation are shown in Figure 1. The tunnel was modelled as a rectangular prism with length L=90 m, width W=5.4 m and height H=2.4 m, with the fire source located 40 m from the entry. In this study, the maximum HRR is approximately 2 MW, and the characteristic length of the fire plume [14] is in an order of 1.5 m. An adequate resolution of the fire plume in large-scale can be achieved with a spatial resolution of about 0.15 m. Grid refinement studies were performed with the extra grid points being added in regions of high velocity or temperature gradients. In the first case, the calculations were performed using a computational mesh with 190 cells along the tunnel (x), 50 cells across (y) and 34 cells in the vertical direction (z). In the second case, the calculations were performed using a computational mesh with 230 cells along the tunnel length (x), 66 cells across (y) and 50 cells in the vertical direction (z). Along the tunnel length, x, start at 0.1 m in the combustion zone, and stretch to about 1 m at the free boundary. In the transversal direction, y, cell sizes are about 0.05 m around the burning zone and stretch to about 0.15 m near the tunnel wall. A uniform grid is used with cell size of about 0.05 m in the z direction. As an illustration, Figures 2 and 3 shows a comparison of the predicted temperature and velocity obtained from the two grid systems at the three locations (upstream, at the fire source and downstream) for U_0=0.85 m/s. It is found that the changes in the calculated plots of the temperature and velocity were relatively small, except at the fire source base, between the two grid systems. A further reduction in the grid size results in a significant reduction in the time step (Δt <0.001 s) for satisfying the CFL stability condition. Moreover, in a LES calculation, commutation of the filtering operation with temporal and spatial differentiation is only strictly valid for uniform grid system. However, a uniform grid system severely restricts its range of applicability to a small-scale fire in 3D simulation. With the use of an extremely fine grid size from a highly compressed grid system, build-up of numerical error could produce spurious results over the course of a LES calculation. Up to now, investigations of the large-scale fire are limited to computations on relatively coarse meshes everywhere. It can be concluded that the

grid system, 250(x) x 34(y) x 48(z), offered the best tradeoff between accuracy and cost for the present purpose.
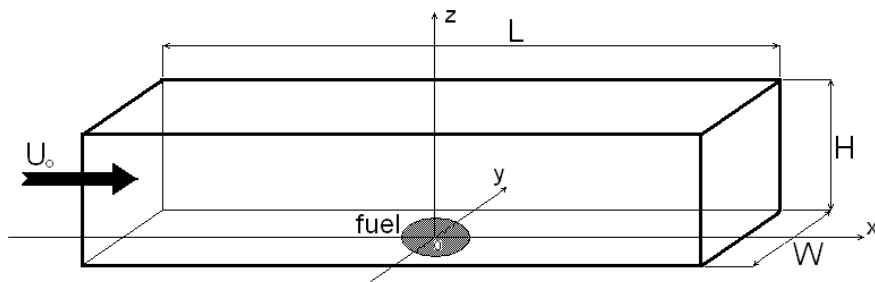

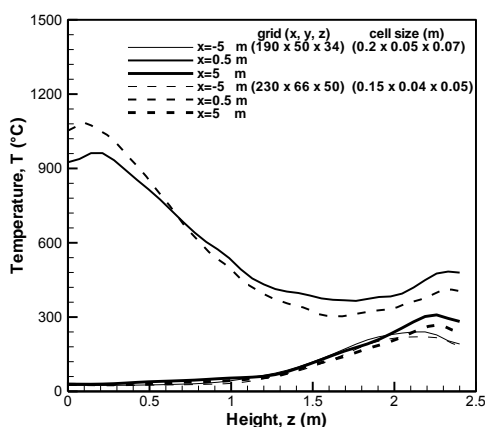Figure 1. Full-scale tunnel fire geometry and the coordinate system

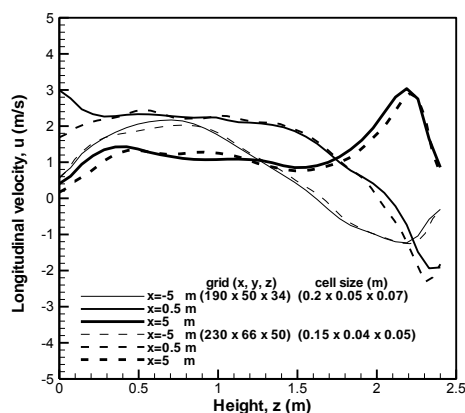Figure 2. Influence of number of grid cells on the predicted temperature

Figure 3. Influence of number of grid cells on the predicted axial velocity

The SGS energy is normally much less than the total kinetic energy and varies with the grid resolution. In the work of Chen et al. [23], a stepwise turbulent energy cascade is supposed to take place from mean flow down to Kolmogorov scale, which is applicable only to small-scale fire. In the current model, the turbulent mixing rate is calculated by directly replacing the total kinetic energy with the subgrid scale properties. This minimizes computational expense because it avoids calculating the turbulent energy cascade up to Kolmogorov scale. The profiles of the mean temperature and the axial velocity versus radial position obtained from the cascade concept of Chen [23] and the current EDC are compared with the experimental data in Figs.4 and 5. The comparison of model predictions with experimental data allows to conclude that in most fires, the primary momentum transport of turbulent diffusion flame is sustained by large-scale energy-containing eddies [19].

There are still very few experimental data available about CO and soot concentrations from a full-scale tunnel fire, due to the high cost and instrumentation difficulty. Molecular species concentrations from a propane pool fire of 0.75 m in diameter with 178 kW has been measured by Orloff [12]. A numerical simulation in such conditions was performed with an uniform grid system (2 cm) containing 70(x) x 70(y) x 100(z) cells. Evident in Fig.6 is the good agreement between the predicted and measured CO_2 species concentration in radial traverse. We have plotted CO predicted in a traverse versus radial position at z=0.12 m and at the centreline against the average mixture fraction, Z. It can be seen from data shown in Fig.7 that the peak magnitude of the CO is predicted relatively well, and the predicted profiles exhibit a high degree of similarity that is observed experimentally. The soot volume fraction versus radial position at z= 0.12 m above a propylene pool fire [12] is shown in Fig.8. The radial locations of the soot volume fraction line up well with those measured experimentally. We have plotted also the soot volume fraction against the mixture

fraction at the centreline in Fig.9. It is found that the agreement between the computation and experiment is better in the flame close to the fuel-rich condition (Z>0.1) at a high temperature region where soot formation is likely subject to precursors. Past the flame tip (Z<0.06), the computed soot is particularly low than the experimental one. The measurements show that fuel-lean conditions generally exhibit low concentration of soot (cf. Fig.8) in the radial direction, which differ from the observations of soot emission at the centreline (cf. Fig.9). This is expected because, at the flame tip, soot surface growth continues after its oxidation has ceased, causing the higher soot volume fraction to be sustained for a small mixture fraction. Both the experiment and prediction show no correlation of soot concentration in terms of the mixture fraction, which suggests that soot formation in turbulent pool fires is fundamentally controlled by transient chemical kinetic processes. Buoyant turbulent diffusion flames, such as tunnel fires, generally have modest stretch rates so that local concentration of CO in the fire is correlated solely as a function of mixture fraction. For a given fuel, CO generation is relatively independent of position in the overfire region, of pool diameter and of theoretical HRR. The chemical composition depends mainly on the type of the fuel. This fire model's treatment is sufficiently accurate for predictions of soot and CO concentrations from a tunnel fire.
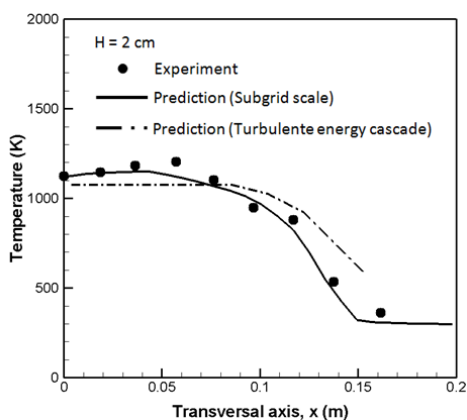
Figure 4. Comparison of the predicted mean temperature to the experiment
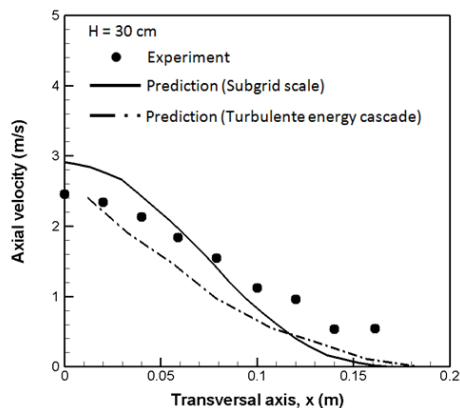
Figure 5. Comparison of the predicted mean axial velocity to the experiment
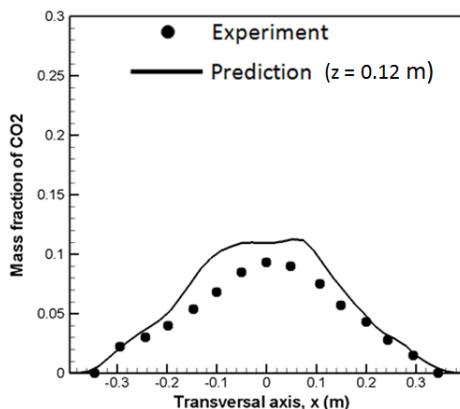
Figure 6. Comparison between the measured and predicted mean CO_2 mass fraction at a height of 0.12 m
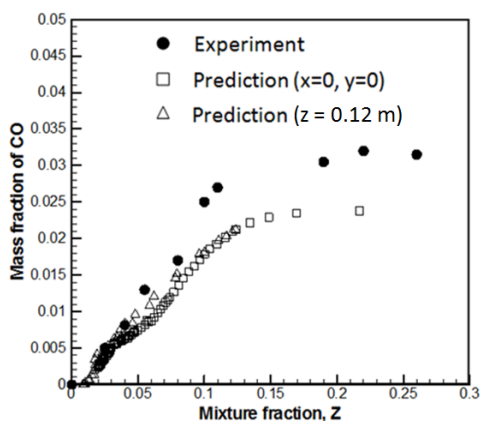

Figure 7. Comparison between the measured and predicted CO mass fraction as a function of the average mixture fraction
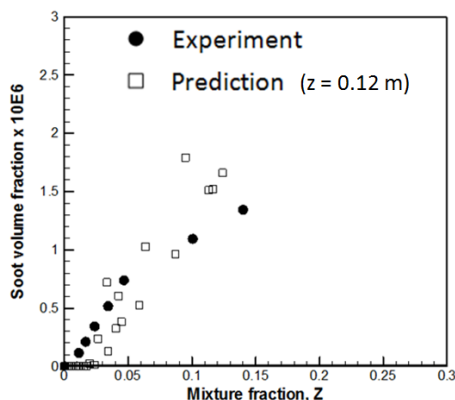
Figure 8. Comparison between the measured and predicted soot volume fraction as a function of the average mixture fraction at z=0.12 m
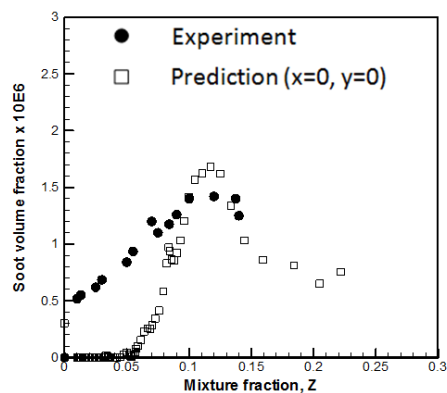
Figure 9. Comparison between the measured and predicted soot volume fraction as a function of the average mixture fraction at the centreline

During the experiment [6], the liquid fuel, octane (C_8H_{18}), is vaporised due to flame heat feedback on its surface on a 2 cm layer of water contained in circular trays. The subsequent burning above the liquid fuel surface couples with the air supply rate. For a pool diameter, D, of 1 m, the experimentally determined values of the mass loss rate of liquid fuel, $\dot{m}_s''$, vary from 0.07, 0.065 to 0.058 kg/m²s as the airflow velocity through the tunnel increases from 0.5, 0.85 to 2 m/s. The predicted mass loss rate of liquid fuel and heat release rate (HRR), both as temporal quantities, are indicated in Figs.10 and 11 for the three airflow conditions. There are still very few experimental data available concerning the temporal evolution of the mass loss rate of liquid fuel for a full-scale tunnel fire considered here. During the fire growth period, the mass loss rate, $\dot{m}_s''$, increases with time, and its magnitude is noticeably higher under practically quiescent conditions (U_0=0.5 m/s). By taking into account the heat loss within the liquid, the transition time required for achieving a steady-state burning rate is about 100 s comparable to the time in the test. The predicted trend of increase in the burning rate from 0.065 to 0.07 kg/m²s in the quasi-steady period with a reduction in the ventilation rate from 0.85 to 0.5 m/s is in agreement with the measured one during the course of the experiment [6]. The worst discrepancy is found to occur for the high ventilation velocity of 2 m/s, and the burning rate is consistently under-predicted by about 10%. In the presence of a strong crossflow, the shear stress at the gas-liquid interface may be large enough to induce internal liquid-phase circulation which enhances the liquid burning rate. These coupling modes can not be accounted for in the present numerical simulation. Temporal data are important in the presentation of the heat flux information, because changes in the burning rate can be correlated with events in the heat flux. In the presence of a crossflow, the burning rates were found to be nonuniform across the pool surface, and the maximum local burning rate was observed at the pool centre. Thus the predicted radiative and convective heat fluxes above the liquid fuel surface at the centre are plotted in Figures 12 and 13 as a function of crossflow speed. As buoyancy controls the flame shape (cf. Fig.18), the radiative heat fluxes suggest an inverse dependence with the ventilation velocity U_0. A monotonous increase of the peak radiation flux from 30, 60 to 90 kW/m² is brought about with a decrease of the ventilation velocity from 2, 0.85 to 0.5 m/s due to increase in the flame thickness above the pool surface. The unsteadiness of convective flux (cf. Fig.13) is most noticeably manifested itself through pulsating motion of the gas volume in the vicinity of the flame. The high ventilation current of 2 m/s bends the plume, but reduction in the gas temperature level above the liquid surface (cf. Fig.18) results in a low convection flux of 7 kW/m². Relative importance of the different mechanisms of heat transfer is estimated. Contribution by radiation is higher than 90% of the total heat flux for the ventilation velocity below 1 m/s, and is about 80% of the total flame feedback for the high velocity of 2 m/s. The mass loss rate is controlled by radiation from the flame which can significantly strength the liquid heating rate during the fire growth period. Under practically quiescent conditions (U_0=0.5 m/s), the liquid surface temperature (cf. Fig.14) rises during the fire growth period, and approaches its boiling point in the quasi-steady period. While for the high airflow of 2 m/s, the heat feedback is momentarily compensated by the vaporization heat, resulting in a practically steady, low surface temperature of about

50°C. All of the trends in the mass loss rate are consistent with those predicted in the heat flux (cf. Figs.12 and 13). The heat release rate (cf. Fig.11) is correlated with the trend of the mass loss rate, and however, no experimental data are available for comparison. Based on a heat of combustion of H_c=44400 kJ/kg, the low airflow velocity (U_o<1 m/s) exhibits the highest HRR of about 2.4 MW, and the high one of 2 m/s, the lowest of about 1.9 MW. This trend emphasizes the importance of considering the induced interaction of fires and crossflow when estimating the global mass loss and heat generation rates.
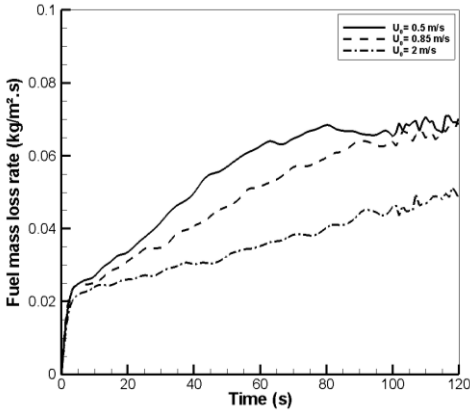
Figure 10. Predicted mass loss rate of liquid fuel
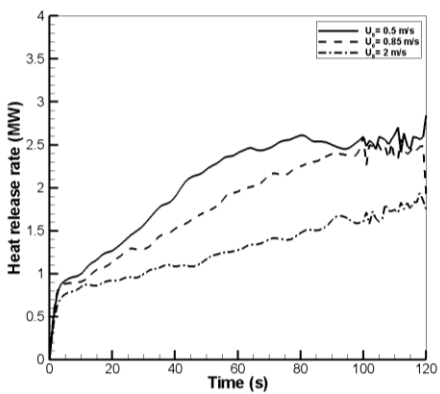
Figure 11. Predicted heat release rate
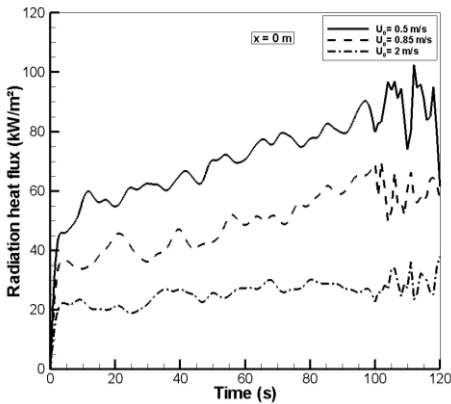
Figure 12. Predicted radiative heat flux above the liquid fuel surface at the centre
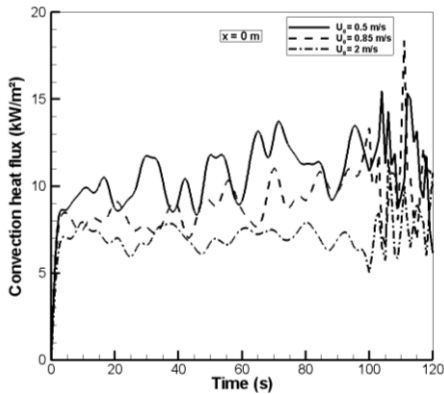
Figure 13. Predicted convective heat flux above the liquid fuel surface at the centre
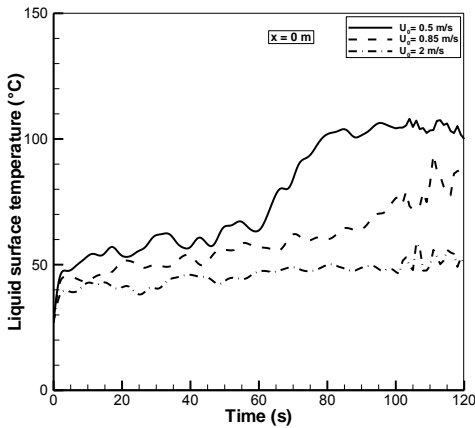
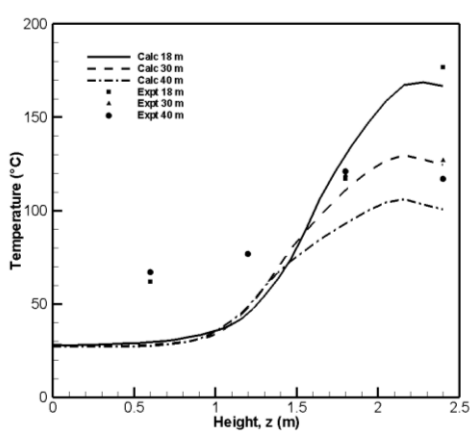Figure 14. Predicted surface temperature of the liquid fuel at the centre

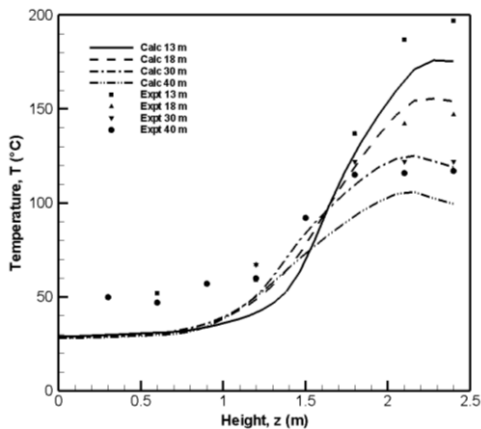Figure 15. Comparison between the calculated and measured temperature at U_o=0.5 m/s

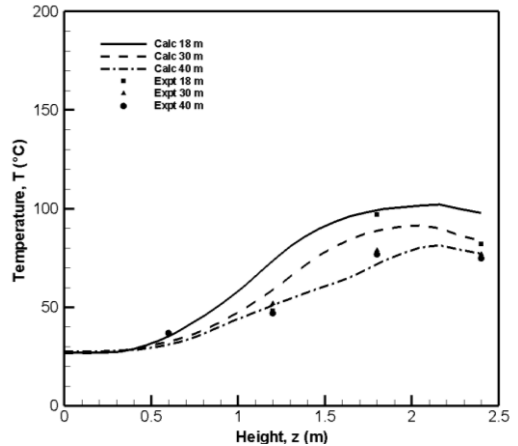Figure 16. Comparison between the calculated and measured temperature at $U_o=0.85$ m/s

Figure 17. Comparison between the calculated and measured temperature at $U_o=2$ m/s

In this work, all the results from the computer outputs were time-averaged from the final 20 seconds in a steady-state period for comparing with the experimental data. The predicted temperature profiles along the height in the smoke region on the axis of the tunnel downstream of the fire are compared with the experimental data in Figs. 15, 16 and 17 for the wind velocity of 0.5, 0.85 and 2 m/s. The computations under-predict the temperature of about 30°C for the low ventilation velocity ($U_0 < 1$ m/s), and consequently, the vertical stratification present in the experiment. A good agreement with the experimentally-determined temperature profiles are obtained for the high ventilation velocity of 2 m/s (cf. Fig.17). Iso-contours of the temperature on the axis of symmetry of the tunnel are shown in Figure 18(a,b,c) for the ventilation rates of $U_0=0.5$, 0.85 and 2 m/s. Inclination of the fires due to cross-flow can be characterized by the angle, α (cf. Fig.18c), formed between the beginning layer of 600°C as a visible flame, and the vertical axis, z (cf. Fig.1). The measured angle, derived from video images with an uncertainty of $\pm 10°$ [6], varies from 46, 56 to 66° with a rise of the ventilation velocity from 0.5, 0.85 to 2 m/s. The calculated angles of fires are 22 and 40° for the ventilation velocity of 0.5 and 0.85 m/s, respectively. A relatively good agreement between the predicted (56°) and measured flame angles is obtained for the high wind velocity of 2 m/s. Globally, the calculated inclination of the fire is less noticeable than the measured one with a rise of the ventilation velocity, probably due to the different definition of the visible flame shape in the simulation and experiment. For a full-scale fire, only the flame video image is available, and the numerical results are limited to a qualitative comparison with the flame video image.
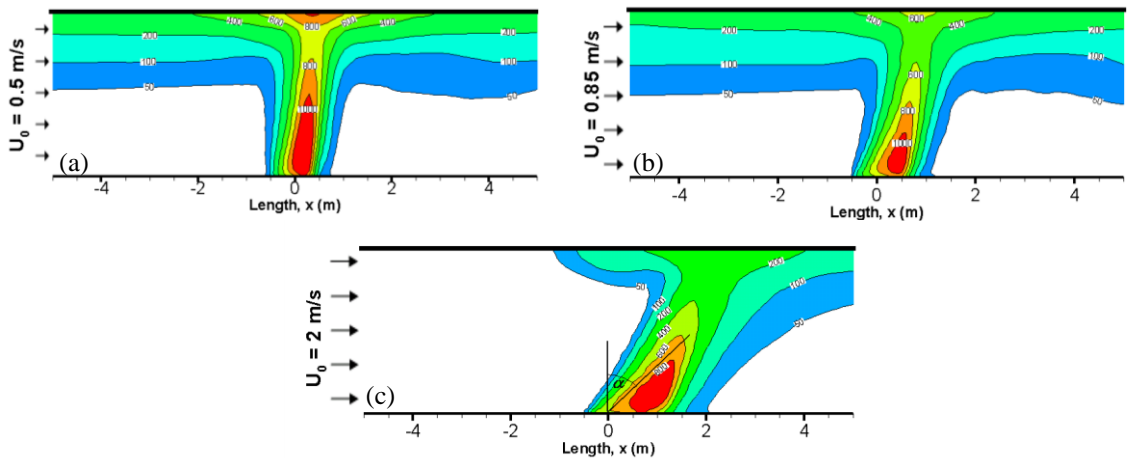

Figure 18. Iso-contours of the predicted temperature (°C)
(a) Ventilation rate of 0.5 m/s; (b) Ventilation rate of 0.85 m/s; (c) Ventilation rate of 2.0 m/s

In a tunnel, after the fire impinges on the ceiling, smoke progressively spreads along the ceiling during the fire growth period, and later attains a thermal steady state. As an illustration, the predicted iso-contours of the time-averaged temperature on the axis of symmetry of the tunnel for U_0=0.85 and 2 m/s are presented in Figure 19(a,b). The calculated extent of the hotter layer (T>50 °C) takes place up to the entrance for U_0<1 m/s. With an increase of the wind velocity to 2 m/s, the ventilation current bends the plume and the length of the ceiling layer flowing against the ventilation is completely suppressed due to the dominant inertia force in the ventilation current. An inverse dependence of back layer length with the airflow velocity is correctly predicted. Iso-contours of the predicted CO and soot mass fractions at the wind velocity of 0.85 and 2 m/s on the axis of symmetry are shown in Figures 20 and 21(a,b). The abundant CO with a mass fraction of 1% is formed around the fire base due to locally under-ventilated condition, and is deflected near the ceiling with presence of a noticeable smoke stratification. When the airflow velocity is low (U_0=0.85 m/s), the back layer flow takes place along the ceiling against the ventilation flow through the buoyancy forces generated by the fire, and receives the same amount of CO and soot as the forward layer. Along the ceiling, the back layer carries the CO with a concentration of 200 ppm, and however, the less soot production (100 ppm). A critical velocity of 2 m/s is required for a fire of 2-2.5 MW to severely suppress CO and soot upstream the fire source due to enough oxygen and turbulence development so that the fire plume tilts forward (cf. Fig.18c). Although a critical ventilation helps to provide enough incoming air flow towards the channel, a high amplitude of the CO and soot concentrations up to 200 ppm is maintained downstream the fire. The conclusion is came that based on the toxic products, a tunnel fire remains dangerous downstream the fire source even at a critical velocity.
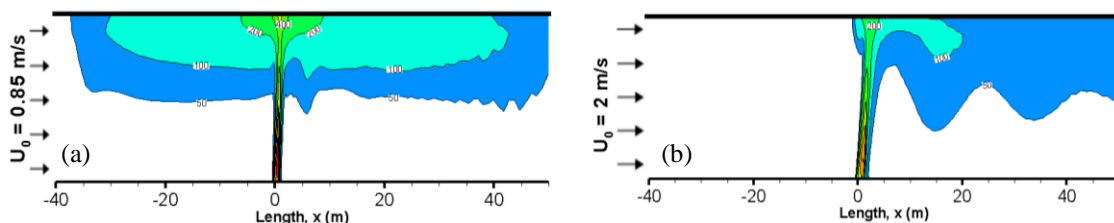

Figure 19. Iso-contours of the predicted temperature (°C) (a) U_0=0.85 m/s; (b) U_0=2 m/s
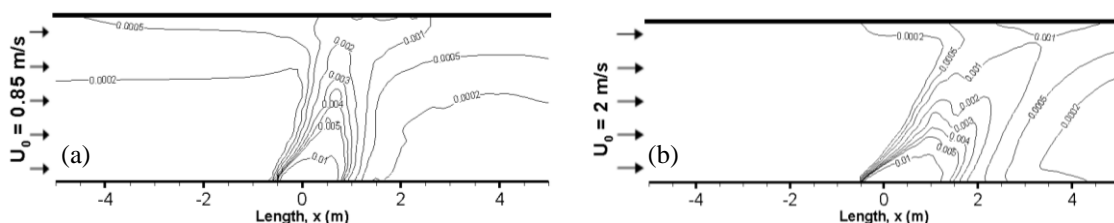

Figure 20. Iso-contours of the predicted CO mass fraction (a) U_0=0.85 m/s; (b) U_0=2 m/s
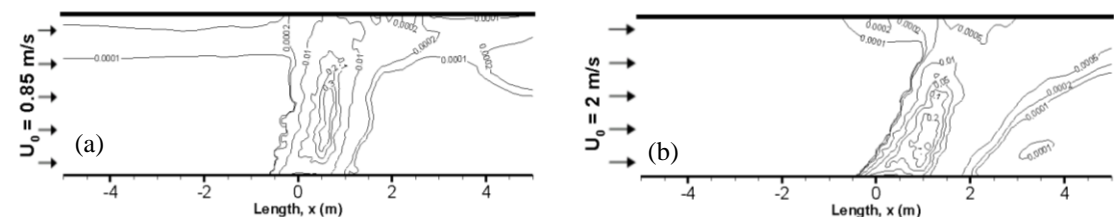

Figure 21. Iso-contours of the predicted soot mass fraction (a) U_0=0.85 m/s; (b) U_0=2 m/s
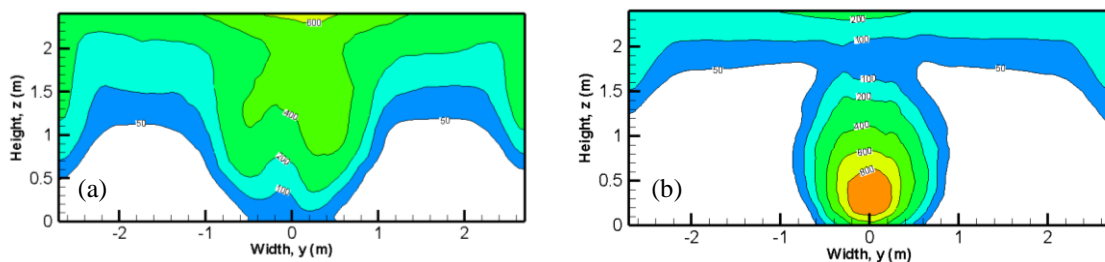
Figure 22. Iso-contours of the predicted temperature (°C) (a) U_0=0.85 m/s; (b) U_0=2 m/s
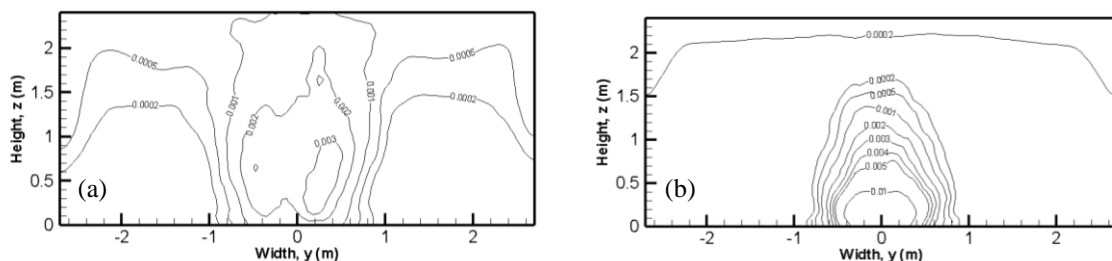

Figure 23. Iso-contours of the predicted CO mass fraction (a) U_0=0.85 m/s; (b) U_0=2 m/s

The 3D phenomena of the tunnel fire can be seen in Figures 22 and 23 (a,b) through iso-contours of the temperature/CO on the cross-stream plane of the flame just downstream the pool (x=1 m). For the low ventilation velocity of 0.85 m/s, there are incoming air flow towards the fire source, and the improving mixing between oxygen and fuel correlates to a weak CO concentration of 0.3% (cf. Fig.23a). The strong streams toward the centre region are visible, and the higher temperature region moves towards the upper corners because of the growth of the recirculation zone. For the strong airflow of 2 m/s, the strength of the re-circulation towards the fire source is significantly reduced, and in the oxygen-lean fuel-rich condition, CO concentration up to 1% (cf. Fig.23b) is formed there. The temperature level and CO production enters rapidly the decay phase once outside the fire source due to enough oxygen and turbulence development.

CONCLUSION

It is felt that Large-eddy simulation coupled with EDC is convenient for simulating a transient fire growth and a progressive vitiation of the ambient medium in a full-scale experimental tunnel. For a self-sustained, large-scale liquid fire, rates of fuel release are controlled by radiation from the flame, and in inversely proportional to the airflow velocity. Validation of the numerical models was carried out for the temperature in the smoke region. The predicted results provide a good agreement in the CO distribution as compared to the experimental data from a pool fire. Conversely, the difference for the soot production between the prediction and experiment is evident in the fuel-lean condition. A reasonably accurate calculation of the thermal/dynamic fields and the toxic production from a large-scale tunnel fire was achieved. Although the smoke-point model is incapable of accurately reproducing soot surface growth, it should be capable of capturing global trends for use in engineering calculations of radiation and visibility from tunnel fires. The model must be further validated to include downward flame spread over a condensed fuel surface, induced by the high temperature of smoke which pose significant threat to inflammable objects exposed downstream the fire source, potentially inducing flashover within tunnel.

REFERENCES

[1] Wu, Y. and Bakar, M.Z.A., (2000) Control of smoke flow in tunnel fires using longitudinal ventilation systems – a study of the critical velocity, Fire Safety 35:363-390, http://dx.doi.org/10.1016/S0379-7112(00)00031-X

[2] Kunsch, J.P., (2002) Simple model for control of fire gases in a ventilated tunnel, Fire Safety 37:67-81, http://dx.doi.org/10.1016/S0379-7112(01)00020-0

[3] Vauquelin, O., (2005) Parametric study of the back flow occurrence in case of a buoyant release into a rectangular channel, Experimental Thermal and Fluid Science 29:725-731, http://dx.doi.org/10.1016/j.expthermflusci.2005.01.002

[4] Rew, C. and Deaves, D., "Fire spread and flame length in ventilated tunnels – a model used in channel tunnel assessments," Proceedings of the International Conference on Tunnel Fires and Escape from Tunnels, Lyon, France, 5-7 May, 1999, pp. 397-406.

[5] Lönnermark, A. and Ingason, H., (2006) Fire spread and flame length in large-scale tunnel fires, Fire Technology 42(4):283-302, http://dx.doi.org/10.1007/s10694-006-7508-7

[6] Fletcher, D.F., Kent, J.H., Apte, V.B. and Green, A.R., (1994) Numerical simulations of smoke movement from a pool fire in a ventilated tunnel, Fire Safety 23:305-325, http://dx.doi.org/10.1016/0379-7112(94)90033-7

[7] Woodburn, P.J. and Britter, R.E., (1996) CFD simulations of a tunnel fire-Part I, Fire Safety 26:35-62, http://dx.doi.org/10.1016/0379-7112(96)00018-5

[8] Hwang, C.C. and Edwards, J.C., (2005) The critical ventilation velocity in tunnel fires – a computer simulation, Fire Safety 40:213-244, http://dx.doi.org/10.1016/j.firesaf.2004.11.001

[9] Babrauskas, V., (1998) A methodology for obtaining and using toxic potency data for fire hazard analysis, Fire Safety 31:345-358, http://dx.doi.org/10.1016/S0379-7112(98)00013-7

[10] Gottuk, D.T., Rohy, R.J. and Beyler, C.I., "Study of carbon monoxide and smoke yields from compartment fires with external burning," Proceedings of the 24th Symposium (International) on Combustion. Pittsburgh : The Combustion Institute, 1992, pp.1729-1735.

[11] Koylu, U.O. and Faeth, M., (1991) Carbon monoxide and soot emissions from liquid fuelled buoyant turbulent diffusion flames, Combustion and Flame 87:61-76, http://dx.doi.org/10.1016/0010-2180(91)90027-9

[12] Orloff, L. J. de Ris and Delichatsios, M.A., (1987) Chemical effects on molecular species concentrations in turbulent fires, Combustion and Flame 69:273-289, http://dx.doi.org/10.1016/0010-2180(87)90121-0

[13] Wen, Z., Yun, S., Thomson, M.J. and Lightstone, M.F., (2003) Modeling soot formation in turbulent kerosene/air jet diffusion flames, Combustion and Flame 135:323-340, http://dx.doi.org/10.1016/S0010-2180(03)00179-2

[14] Floyd, J.E. and McGrattan, K.B., (2009) Extending the mixture fraction concept to address under-ventilated fires, Fire Safety 44:291-300, http://dx.doi.org/10.1016/j.firesaf.2008.07.002.

[15] Miloua, H., Azzi and Wang, H.Y., (2011) Evaluation of different numerical approaches for a ventilated tunnel fire, Fire Sciences 29(5) 403-429, http://dx.doi.org/10.1177/0734904111400976

[16] Beji, T., Zhang, J. and Delichatsios, M.A., (2008) Determination of soot formation rate from laminar smoke point measurements, Combution Science and Technology 180(5):927-940, http://dx.doi.org/10.1080/00102200801894398

[17] Menon, S., Yeung, P.K. and Kim, W.W., (1996) Effect of subgrid models on the computed interscale energy transfer in isotropic turbulence, Computers and Fluids 25:165-176, http://dx.doi.org/10.1016/0045-7930(95)00036-4

[18] Dryer, F.L. and Glassman, I., "High-temperature oxidation of CO and CH4," Proceedings of the 14th Symposium (International) on Combustion. Pittsburgh : The Combustion Institute, 1972, pp.987-1003.

[19] Baum, H.R. McGrattan K.B. and Rehm, R.G., (1997) Three dimensional simulation of fire plume dynamics, Heat Transfer Society of Japan 35(139) 45-52.

[20] Adiga, K. C. and Ramaker, D.E., (1989) Modeling pool-like gas flames of propane, Fire Safety 14: 241-250, http://dx.doi.org/10.1016/0379-7112(89)90058-1

[21] Djilali, N., Gartshore, I. and Salcudean, M., (1989) Calculation of convective heat transfer in recirculating turbulent flow using various near-wall turbulence models, Numerical Heat Transfer 16:189-212, http://dx.doi.org/10.1080/10407788908944713

[22] Murty Kanury, A., *Introduction to Combustion Phenomena*, New York: Gordon, ISBN 0-677-02690-0, 1984, p.142.

[23] Chen, Z.B., Wen, J.X., Xu B.P. and Dembele, S., "The extension of eddy dissipation concept in the framework of Large Eddy Simulation and the subsequent modification," *23rd ICDERS*, 2011, Irvine, USA.